SnO$_2$ Nanostructures: Effect of Processing Parameters on Their Structural and Functional Properties

Tetiana A. Dontsova[*], Svitlana V. Nagirnyak, Vladyslav V. Zhorov and Yuriy V. Yasiievych

Abstract

Zero- and 1D (one-dimensional) tin (IV) oxide nanostructures have been synthesized by thermal evaporation method, and a comparison of their morphology, crystal structure, sorption properties, specific surface area, as well as electrical characteristics has been performed. Synthesized SnO$_2$ nanomaterials were studied by X-ray diffraction, scanning and transmission electron microscopy (SEM and TEM), N$_2$ sorption/desorption technique, IR spectroscopy and, in addition, their current-voltage characteristics have also been measured. The single crystalline structures were obtained both in case of 0D (zero-dimensional) SnO$_2$ powders and in case of 0D nanofibers, as confirmed by electron diffraction of TEM. It was found that SnO$_2$ synthesis parameters significantly affect materials' properties by contributing to the difference in morphology, texture formation, changes in IR spectra of 1D structure as compared to 0D powders, increases in the specific surface area of nanofibers, and the alteration of current-voltage characteristics 0D and 1D SnO$_2$ nanostructures. It was established that gas sensors utilizing of 1D nanofibers significantly outperform those based on 0D powders by providing higher specific surface area and ohmic I–V characteristics.

Keywords: Tin (IV) oxide, Thermal evaporation method, 0D nanostructures, 1D nanostructures, I–V curves

Background

Tin (IV) oxide (SnO$_2$) is a typical *n*-type semiconductor with a wide direct band gap of 3.6 eV [1]. SnO$_2$ exhibits a number of interesting functional properties such as optical transparency in the visible spectrum [2], chemical stability at high temperatures [3], good surface adsorption properties of oxygen and availability of numerous oxygen species and active acid sites on its surface [4], high specific theoretical capacity [5], and excellent electrical characteristics [3, 6]. As a result, SnO$_2$ is broadly used as a part of catalysts for oxidation of organic compounds [4, 7], as an anode material in lithium-ion batteries [5], as transparent electrodes in solar cells [8], as a host material and a buffer layer in many optoelectronic devices [9], or as a sensitive layer in gas sensors to detect harmful for human health and hazardous gases such as CO, NO$_x$, H$_2$S, H$_2$, and CH$_4$. [10–13]. Today, the development of superior gas sensors is extremely important because they not only allow safely controlling the environment at home and industrial settings [12] but also provide an easy diagnostic tool for detection of early stages of otherwise hard or impossible to detect diseases at air exhalation among other applications [14].

It was established [15] that nanostructured SnO$_2$ provides far better gas sensing properties as compared to SnO$_2$ micron size materials. Thermal evaporation [16], hydrothermal synthesis [17], sol-gel method [18, 19], template synthesis [20], and laser ablation [21] are the most explored methods for synthesis of SnO$_2$ nanostructures. Thermal evaporation method is the most promising technique as it allows to produce single crystalline 0D (zero-dimensional) or 1D (one-dimensional) SnO$_2$ nanoparticles with high specific surface area and excellent gas sensing properties [16, 22].

There are many papers recently published that study either 0D or 1D nanostructured SnO$_2$ [15, 16, 23, 24]. However, the direct comparison of performance of these structurally very different materials is lacking. Therefore, the goal of this paper is to fill the gap by providing a comparison of structural and functional behavior of 0D and 1D SnO$_2$ nanostructures.

* Correspondence: dontsova@ua.fm; dontsova@xtf.kpi.ua
Department of Chemistry, National Technical University of Ukraine "Igor Sikorsky KPI", Kyiv 03056, Ukraine

Dontsova *et al. Nanoscale Research Letters* (2017) 12:332

Page 2 of 7

Methods

Materials Synthesis

Tin (II) oxalate (SnC_2O_4), prepared by sol-gel method from tin (II) chloride ($SnCl_2$) and ammonium oxalate ((NH_4)$_2C_2O_4$) as in [10], was used as a precursor for the SnO_2 synthesis. For the synthesis of 0D and 1D SnO_2 nanostructured materials, 2 g of SnC_2O_4 powder was loaded into $50 \times 10 \times 10$ mm alumina boat each, which were placed inside of a quartz tube in two different horizontal-type furnaces. Two furnaces had identical settings with the only exception that one furnace provided faster heating rate of 80 K/min, and a second furnace provided only 20 K/min heating rate. The N_2 gas with 0.005% O_2 impurity content was used as an inert atmosphere that was supplied to the quartz tube before heating began [10, 22]. Both furnaces were heated to 1123 K and kept at this temperature for dwell time of 1 h. After finishing of synthesis procedure, furnaces were turned off and cooled naturally. As a result of the thermal evaporation, the nanocrystalline SnO_2 was obtained due to following reactions [22]:

$$SnC_2O_4 \rightarrow SnO + CO + CO_2,$$
$$SnO \rightarrow SnO_2 + Sn,$$
$$Sn + O_2 \rightarrow SnO_2.$$
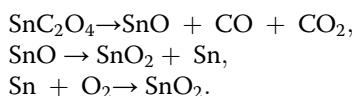
The SnO_2 sample with the fast heating rate was marked as TO1, and the SnO_2 sample with slow heating rate was named TO2.

Characterization Techniques

In X-ray diffractometer Ultima IV (Rigaku, Japan) with CuKα radiation at 40 kV, 30 mA was used to collect diffraction patterns of the SnO_2 samples. The powdered samples were scanned from 20 to 80 2θ at 1°/min with a scanning step of 0.0001°. XRD patterns were analyzed by the PDXL software package using database ICDD/PDF-2 and COD. The crystalline size and lattice parameters of the materials were calculated automatically by the software.

Both Transmission Electron Microscopy PEM 100–01 (Selmi, Ukraine) and Scanning Electron Microscopy REM 106I (Selmi, Ukraine) were used for characterization of particle's size and morphology of the obtained SnO_2 samples.

Specific surface area of the samples was studied by adsorption/desorption of nitrogen (Quantachrome® Autosorb, Quantachrome Instruments, USA) using Langmuir isotherm and Brunauer-Emmett-Teller (BET)-based software.

IR 4000–400 cm^{-1} wavenumber spectra of SnO_2 were collected using FTIR spectrometer (Thermo Nicolet Nexus FTIR, Thermo Fisher Scientific, USA). For spectra collection, SnO_2 samples were mixed with pre-dried KBr (for spectroscopy, "Aldrich," USA) at 1:30 SnO_2/KBr ratio.

Measurements of current-voltage characteristics of SnO_2 nanostructures were carried by using gas sensors developed utilizing a special test structures. A $6 \times 10 \times 2$ mm crystalline glass ceramic material (Sitall, Ukraine) [25] was used as a substrate upon which the interdigitated Ni electrodes were deposited by a thermal evaporation technique (Fig. 1). As a result of the deposition, Ni electrodes with 50 μm width 50 and 400 μm thickness were produced. After electrode deposition, the copper wires covered with silver and coated by Teflon were connected to the contact pads by soldering using common lead-bearing solder (60% tin; 40% lead). After that, the SnO_2 material was deposited on the top of the Ni electrodes. The deposition of sensitive layer was performed by the sedimentation on the surface of electrodes. For this purpose, SnO_2 1 g/cm^3 suspension in ethanol was prepared and stirred in ultrasound bath for 90 s, after which the complete test structure with deposited interdigitated Ni electrodes, contact pads and parts of Cu wires was fully immersed into the suspension and left overnight to achieve a complete liquid evaporation. After the deposition of SnO_2 layer on Ni-interdigitated electrodes of the test structure, the gas sensor was produced.

The block diagram of the electrical circuit with resistance connected in parallel used to measure the electrical
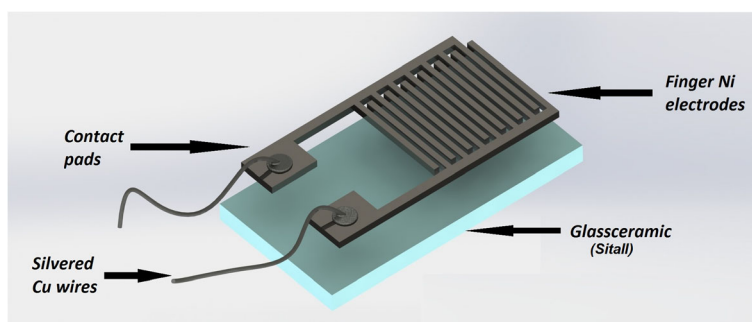

Fig. 1 A schematic presentation of gas sensor's test structure used for I–V measurements of SnO_2

Dontsova *et al. Nanoscale Research Letters* (2017) 12:332

Page 3 of 7

properties of gas sensors are shown in Fig. 2. The electrical circuit consists of the power supply, voltmeter, model resistance, and actually gas sensor test structure. During current-voltage measurements, the gas sensor was placed inside of the tube furnace, and measurements were performed at three different temperatures (323, 372, and 423 K) in 5–30 V voltage range at ambient.

Results and Discussion
X-ray Diffraction

X-ray diffraction patterns for two SnO_2 nanostructured materials are shown in Fig. 3, where the first diffraction pattern was collected using SnO_2 synthesized at 80 K/min faster heating rate (Fig. 3a), while a second diffraction pattern was obtained from SnO_2 synthesized at the same synthesis conditions, but using 20 K/min slower heating rate (Fig. 3b). As it was expected, in both cases, SnO_2 nanostructures were crystallized in tetragonal *P42/mnm* space group with identical a = 4.74 Å, c = 3,19 Å lattice parameters, which correspond well with the lattice of tetragonal SnO_2 reported in JCPDF No 41-1445 [26]. The average crystallite size calculated automatically by PDXL software from the FWHM of all peaks located between 20 and 120 2θ using Scherrer equation was equal to 80.7 and 74.3 nm for SnO_2 with faster and slower heating rates, respectively. At the same time, the difference in heating rates during thermal evaporation synthesis affected not only crystallite size but also the X-ray peals intensity in SnO_2 XRD patterns, especially in 1D nanostructured SnO_2 causing texture formation resulting in the preferred orientation of the certain crystallographic directions. While isotropic material shows 100/75 ratio in (110) and (101) peaks of SnO_2 [26], the SnO_2 synthesized at faster heating rate of 80 K/min shows 100/95 ratio of two major
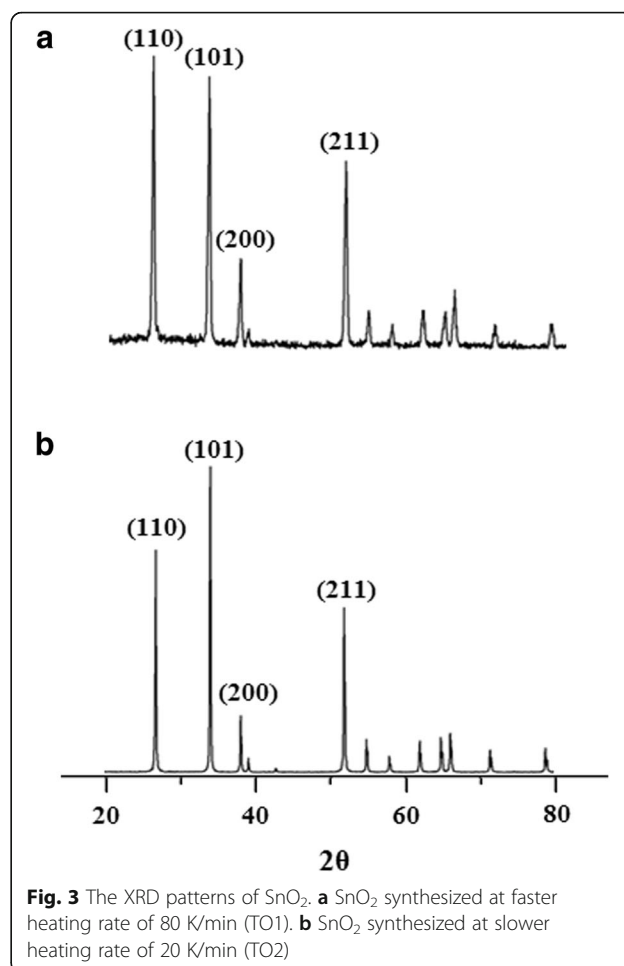
Fig. 3 The XRD patterns of SnO_2. **a** SnO_2 synthesized at faster heating rate of 80 K/min (TO1). **b** SnO_2 synthesized at slower heating rate of 20 K/min (TO2)

hkl peaks; however, for SnO_2 synthesized at slower heating rate of 20 K/min, the (110)/(101) peak intensity significantly reversed to 100/125, thus this nanostructure has a strong preferred orientation of growth in <110> crystallographic direction. Therefore, even based on the analysis of X-ray diffraction patterns of SnO_2 synthesized at different heating rates, one can conclude that the preferred orientation of the material is different and this will certainly affect the morphology of the SnO_2.

Electron Microscopy

TEM microphotographs of SnO_2 samples processed at two different heating rates are shown in Fig. 4. As one can see from Fig. 4, the SnO_2 sample synthesized at 80 K/min fast heating rate (Fig. 4a) has uneven round shape of the particles with an average diameter of 50–150 nm. This measured particle size coincides perfectly with the crystallite size of 80.7 nm calculated from FWHM of the XRD peaks for this material. The selected area electron diffraction (SAED) image of the
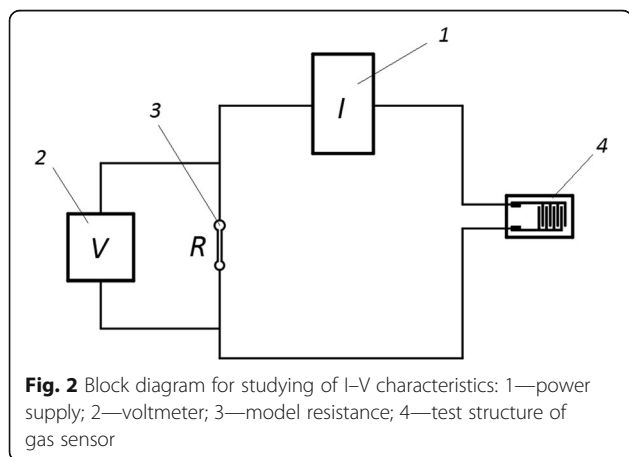
Fig. 2 Block diagram for studying of I–V characteristics: 1—power supply; 2—voltmeter; 3—model resistance; 4—test structure of gas sensor
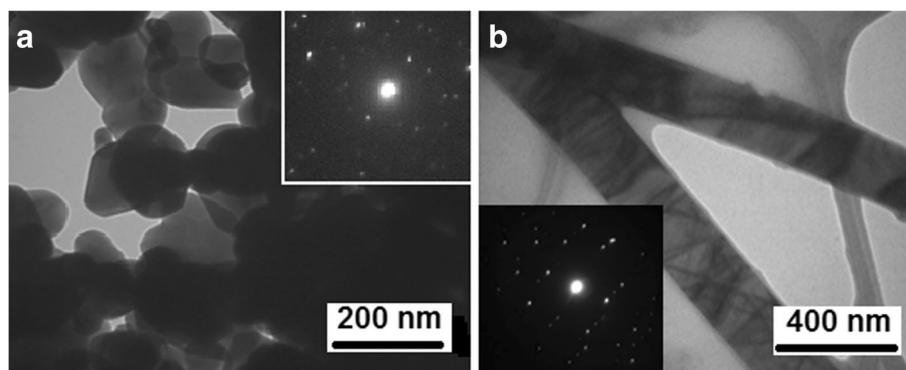
Fig. 4 TEM images of SnO_2 samples. **a** SnO_2 synthesized at faster heating rate of 80 K/min (TO1). **b** SnO_2 synthesized at slower heating rate of 20 K/min (TO2)

particles (Fig. 4a, insert) indicated that those are single crystalline particles. At the same time, the SnO_2 sample synthesized at 20 K/min slow heating rate (Fig. 4b) has long and extended shapes, essentially forming 1D structures. The SAED of 1D structures also shows the crystalline nature of the material (Fig. 4b, insert), and the quality of the SAED pattern is better for 1D SnO_2 fibers in comparison with SnO_2 particles partially because of better crystallinity of the material and partially because only two fibers were used for SAED pattern collection, unlike for the case when many particles contributed to SAED pattern for the SnO_2 powder.

The Specific Surface Area

Table 1 contains results of the structural characteristics of SnO_2 synthesized at faster heating rate of 80 K/min (TO1) and SnO_2 synthesized at slower heating rate of 20 K/min (TO2). Pursuant to these data, the 1D SnO_2 has specific surface area five times higher than 0D SnO_2. Thus, the ratio of surface to volume really increases in the 1D nanostructures as compared with 0D particles.

Also, based on the data in Table 1 and isotherms of nitrogen sorption/desorption (Fig. 5), both SnO_2 samples are non-porous; they are consistent with the results of electron diffraction and microscopy. The revealed negligible porosity was caused by gaps between the primary particles (Table 1). In addition, the formed porous system from particles of 1D nanostructures is characterized

by smaller dimensions than the porous system from 0D particles. This is evidenced by the hysteresis loop in isotherm of 1D nanostructures and the value of the average conditional pore radius for both samples.

IR Spectroscopy

The infrared spectra of two SnO_2 nanostructured samples are shown in Fig. 6. It is known from the analysis of literature (Table 2) that the vibrational bands of the SnO_2 are divided into different regions where both vibrations of SnO_2 atomic structure and vibration of absorbed species such as O_2, CO_2, and even H_2O could be detected. The stretching and antisymmetric Sn–O, Sn–O–Sn, and O–Sn–O vibrations of SnO_2 can be found in the range of 400–1050 cm^{-1}, while absorbed O_2 and CO_2 molecule vibrations are located between 1050 and 3000 cm^{-1} region and physically absorbed water vibrational bands could be found at 3390–3413 cm^{-1} (Table 2). IR spectra presented in Fig. 6 correspond well with the results published in the literature, especially since the 563 cm^{-1} band present in the 1D SnO_2 nanostructure in the current study was also reported to exist in 1D structures by others [23]. The presence of this extra absorption band in the 560–570-cm^{-1} region is known as a characteristic feature of 1D SnO_2 structures, but the nature of their presence still requires clarifications.

I–U Measurements

To study the influence of morphology on electrical properties, I–V curves for 0D and 1D SnO_2 nanostructures were measured. Figure 7 shows I–V curves at 323, 373, and 423 K in range of 5–30 V.

As seen on Fig. 7, the current-voltage curves of these samples are different. For 0D SnO_2 sample, I–V curves are non-ohmic at all temperatures while 1D tin (IV) oxide sample is characterized by linear (ohmic) current-voltage dependences. The various nature of curves for

Table 1 Structural characteristics of sample SnO_2

Characteristics	TO1	TO2
S (m^2/g)	10.6	54.8
The total pore volume (cm^3/g)	0.076	0.065
The average conditional pore radius (nm)	144	24

Dontsova *et al. Nanoscale Research Letters* (2017) 12:332
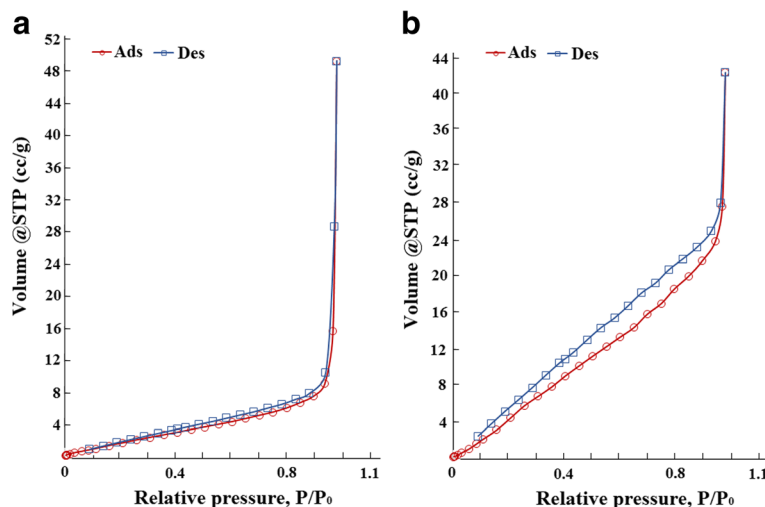
Page 5 of 7

Fig. 5 The sorption isotherm of SnO_2 samples. **a** SnO_2 synthesized at faster heating rate of 80 K/min (TO1). **b** SnO_2 synthesized at slower heating rate of 20 K/min (TO2)

0D and 1D nanostructures related to the different surface to volume ratios. Change in this ratio leads to a change in the I–V behavior of the material. It is known that both surface and bulk conductivities of the SnO_2 contribute to the overall conductivity.

In addition, it is known that the ohmic behavior of current-voltage characteristics is very important for the sensing properties of the material, as the sensing properties of SnO_2 are significantly improved if the material is showing ohmic type semiconducting behavior [27]. Therefore, 1D nanostructures are more desirable for use in gas sensors.

Conclusions

The single crystalline particles of SnO_2 of different morphology (zero-dimensional (0D) and one-dimensional
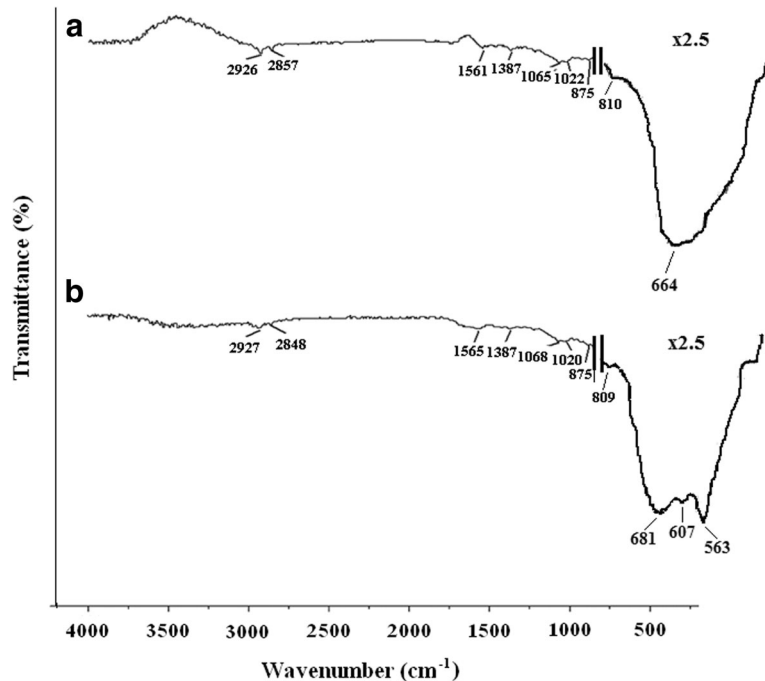

Fig. 6 IR spectra of tin (IV) oxide samples. **a** SnO_2 synthesized at faster heating rate of 80 K/min (TO1). **b** SnO_2 synthesized at slower heating rate of 20 K/min (TO2)

Table 2 Absorption spectra of synthesized SnO_2 samples

Wavenumber (cm^{-1})		Vibrational band	Reference data (cm^{-1})
TO1	TO2		
435	434	Sn–O (O–Sn–O)	428 [23]
–	563	Sn–O (Sn–OH)	537 [28], 546 [29], 567 [23]
–	607	Sn–O (Sn–O–Sn)	613 [30], 623 [31]
664	684	Sn–O	673 [23]
810	809	O–Sn–O	817 [32]
875	875	O–Sn–OH	866 [33]
1022	1020	Sn–O (O–Sn–O)	1021 [34]
1065	1068	O_2^- (chemical adsorption)	1045 [34]
1387	1387	CO_2 (physical adsorption)	1386 [35]
1561	1565	O_2 (physical adsorption)	1580 [34]
–	–	H_2O (bounded) (Sn–OH)	1631 [31], 1633 [31]
2857	2848	CO_2 (chemical adsorption)	2840, 2925 [34]
2926	2927		
–	–	H_2O (adsorbed) (Sn–OH)	3394 [28, 31], 3413 [28]

(1D) nanostructures) were obtained by thermal evaporation method. Such significant difference in the morphology of the SnO_2 nanostructures were achieved due to their different synthesis conditions, as it was found that slower heating rate during the thermal evaporation brings changes to the SnO_2 morphology allowing to receive 1D nanofibers. The comparison of different properties of 0D and 1D SnO_2 nanostructures is presented. It was determined that the morphology has significant impact on the structural and functional properties of SnO_2 as it is reflected in changes in crystal structure where texture formation was recorded, variation of IR spectra, as well as different I–V characteristics of gas sensors based on 0D and 1D SnO_2 structures. It was also established that considerable changes in behavior of SnO_2 depends also on surface to volume ratios of nanostructures.

Based on the experimental data, 1D nanostructures are more desirable for use in gas sensors. Further comparative research of 0D and 1D nanostructures will be carried out regarding sensory properties.
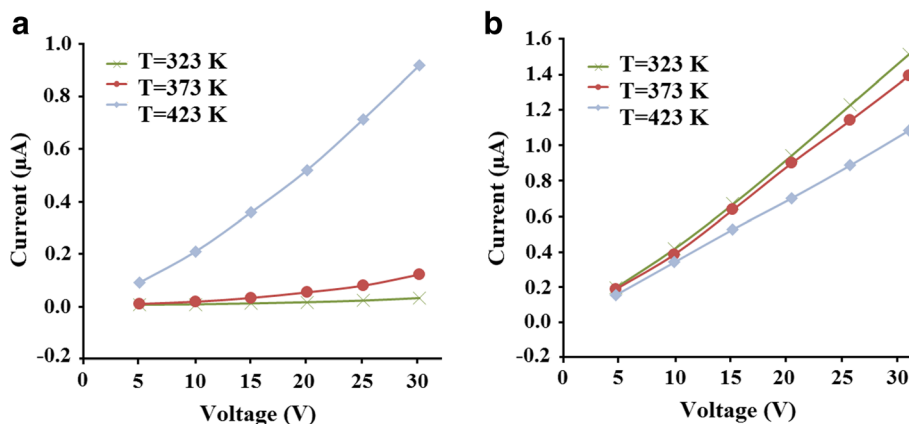

Fig. 7 I–V curves of SnO_2 samples. **a** SnO_2 synthesized at faster heating rate of 80 K/min (TO1). **b** SnO_2 synthesized at slower heating rate of 20 K/min (TO2)

Dontsova *et al. Nanoscale Research Letters* (2017) 12:332

Page 7 of 7

Publisher's Note
Springer Nature remains neutral with regard to jurisdictional claims in published maps and institutional affiliations.

References
1. Munnix S, Schmeits M (1982) Surface electronic structure of tin (IV) oxide. Solid State Commun 43:867
2. Sanon G, Rup R, Mansingh A (1991) Band-gap narrowing and band structure in degenerate tin oxide (SnO_2) films. Phys Rev B Condens Matter 44(11):5672–5680
3. Tan L, Wang L, Wang Y (2011) Hydrothermal synthesis of SnO_2 nanostructures with different morphologies and their optical properties. J Nanomater 2011:1–10
4. Xu X, Zhang R, Zeng X, Han X, Li Y, Liu Y, Wang X (2013) Effects of La, Ce, and Y oxides on SnO_2 catalysts for CO and CH_4 oxidation. ChemCatChem 5:2025–2036
5. Lee S-Y, Park K-Y, Kim W-S, Yoon S, Hong S-H, Kang K, Kim M (2016) Unveiling origin of additional capacity of SnO_2 anode in lithium-ion batteries by realistic ex situ TEM analysis. Nano Energy 19:234–245
6. Janotti A, Varley JB, Lyons JL, Van de Walle CG (2011) Controlling the conductivity in oxide semiconductors. In: Functional metal oxide nanostructures (springer series in materials science), vol 149., pp 23–35
7. Liberkova K, Touroude R (2002) Performance of Pt/SnO2 catalyst in the gas phase hydrogenation of crotonaldehyde. J Mol Catal A Chem 180:221–230
8. Ray S, Dutta J, Barua AK (1991) Bilayer SnO_2:In/SnO_2 thin films as transparent electrodes of amorphous silicon solar cells. This Solid Films 199(2):201–207
9. Tran V-H, Ambade RB, Ambade SB, Lee S-H, Lee I-H (2017) Low-temperature solution-processed SnO_2 nanoparticles as a cathode buffer layer for inverted organic solar cells. ACS Appl Mater Interfaces 9(2):1645–1653
10. Nagirnyak SV, Lutz VA, Dontsova TA, Astrelin IM (2016) Synthesis and characterization of Tin (IV) oxide obtained by chemical vapor deposition method. Nanoscale Res Lett 11(1):343
11. Salehi A (2003) A highly sensitive self heated SnO_2 carbon monooxide sensor. Sensors Actuators B 96:88–93
12. Starke TKH, Coles GSV, Ferkel H (2002) High sensitivity NO_2 sensors for environmental monitoring produced using laser ablated nanocrystalline metal oxides. Sensors Actuators B 85:239–245
13. Ghimbeu CM, Lumbreras M, Schoonman J, Siadat M (2009) Electrosprayed metal oxide semiconductor films for sensitive and selective detection of hydrogen sulfide. Sensors 9:9122–9132
14. Pradhan UU, Bhat P (2015) Breathe analysis for medical diagnostics—a review. Int J Innov Res Dev 4(12):240–246
15. Miller TA, Bakrania SD, Perez C, Wooldridge MS (2006) Nanostructured tin dioxide materials for gas sensor applications. Funct Mater 30:1–24
16. Konga MH, Kwonb YJ, Kwakb DS, Khaib TV et al (2012) The synthesis of crystalline SnO_2 whiskers via a metalorganic chemical vapor deposition process. J Ceram Proc Res 13(6):667–671
17. Chiu HC, Yeh CS (2007) Hydrothermal synthesis of SnO_2 nanoparticles and their gas-sensing of alcohol. J Phys Chem 111:7256–7259
18. Dontsova TA, Ivanenko IM, Astrelin IM, Nagirnyak SV (2014) Stabilization of nanoscale tin (IV) oxide on the surface of carbon nanotubes. J Electr Eng 2(1):34–39
19. Ivanenko IN, Dontsova TA, Astrelin IM, Trots VV (2016) Low-temperature synthesis, structure-sorption characteristics and photocatalytic activity of TiO_2 nanostructures. J Water Chem Technol 38(1):14–20
20. Farrukh MA, Heng BT, Adnan R (2010) Surfactant-controlled aqueous synthesis of SnO_2 nanoparticles via the hydrothermal and conventional heating methods. Turk J Chem 34:537–550
21. Yang H, Song X, Zhang X, Ao W, Qui G (2003) Synthesis and characyerization of SnO_2 nanoparticles for carbon absorbing applications. Mater Lett 57:3124–3127
22. Nagirnyak S, Lutz V, Dontsova T, Astrelin I (2016) The effect of the synthesis conditions on morphology of tin (IV) oxide obtained by vapor transport method. Springer Proc Phys 183:331–341
23. Mondal SP (2010) Temperature dependent growth and optical properties of SnO_2 nanowires and nanobelts. Bull Mater Sci 33(4):357–364
24. Chinh N.D., Toan N.V., Quang V.V., Duy N.V., Hoa N.D., Hieu N.V. Comparative NO2 gas-sensing performance of the self-heated individual, multiple and networked SnO2 nanowire sensors fabricated by a simple process. Sensors Actuators B Chem. 2014:7–12.
25. Fedoseeva TI, Sobolev EV, Takher EA (1972) Obtaining mechanically strong acid-resistant and wear resistant sitall grade BL from fused basal. Steklo Keram 1:29–31
26. McCarthy GJ, Welton JM (1989) X-Ray diffraction data for SnO2. An illustration of the new powder data evaluation methods. Powder Diffract 4(3):156–159
27. Zhai T, Fang X, Liao M, Xu X, Zeng H, Yoshio B, Golberg D. (2009) A Comprehensive Review of One-Dimensional Metal-Oxide Nanostructure Photodetectors. Sensors 9(8):6504-6529
28. Amarlic-Popescu D, Bozon-Verduraz F (2001) Infrared studies on SnO_2 and Pd/SnO_2. Catal Today 70:139–154
29. Avila HA, Rodrigues-Paez JE (2009) Solvent effects in the synthesis process of tin oxide. J Non Cryst Solids 355:885–890
30. Mihaiu S, Atkinson I, Mocioiu O, Toader A, Tenea E, Zaharescu M (2011) Phase formation mechanism in the ZnO-SnO2 binary system. Rev Roum Chim 56:465–472
31. Babar AR, Shinde SS, Moholkar AV, Rajpure KY (2010) Electrical and dielectric properties of co-precipitated nanocrystalline tin oxide. J Alloys Compd 505:743–749
32. Gnanam S, Rajendran V (2010) Anionic, cationic and nonionic surfactants-assisted hydrothermal synthesis of tin oxide nanoparticles and their photoluminescence property. Dig J Nanomater Biostruct 5(2):623–628
33. Liu CM, Zu XT, Wei QM (2006) Fabrication and characterization of wire-like SnO_2. J Phys D Appl Phys 39:2494–2497
34. Agekyan VT (1977) SnO2 solid thin films. Phys Status Solidi 43(1):11–42
35. Wang Y, Ramos I (2007) Preparation and electrochemical properties of SnO_2 nanowires. J Appl Phys 102:1–7